Influence of Nanorod Inclusions on Structure and Primitive Path Network of Polymer Nanocomposites at Equilibrium and Under Deformation

5 AUTHORS, INCLUDING:

Robert A Riggleman
University of Pennsylvania
57 PUBLICATIONS **750** CITATIONS

SEE PROFILE

Martin Kröger
ETH Zurich
239 PUBLICATIONS **3,828** CITATIONS

SEE PROFILE

Influence of Nanorod Inclusions on Structure and Primitive Path Network of Polymer Nanocomposites at Equilibrium and Under Deformation

Gregory N. Toepperwein,[†] Nikos Ch. Karayiannis,[‡] Robert A. Riggleman,[§] Martin Kröger,[⊥] and Juan J. de Pablo*[,†]

[†]*Department of Chemical and Biological Engineering, University of Wisconsin, Madison, Wisconsin 53706-1691, United States , [‡]Institute for Optoelectronics and Microsystems (ISOM) and ETSII, Universidad Politécnica de Madrid (UPM), 28006 Madrid, Spain, [§]Department of Chemical and Biomolecular Engineering, University of Pennsylvania, Philadelphia, Pennsylvania 19104, United States, and [⊥]Department of Materials, Polymer Physics, ETH Zurich, CH-8093 Zurich, Switzerland*

Received July 7, 2010

ABSTRACT: Addition of nanoparticles to polymer melts can significantly alter the mechanical properties of the resulting composite systems. Here we address the influence of nanorods on nanocomposite behavior and, in particular, on the entanglement network of the composites through extensive Monte Carlo and molecular dynamics simulations at equilibrium and under uniaxial deformation. Recently proposed topological algorithms are used to determine the primitive path network and the entanglement molecular weight of polymer–rod composites. A systematic study is presented of the effects of particle size, aspect ratio and volume fraction on their structure and entanglement state. For the primitive path analysis we consider two physical cases: the "frozen particle limit" where nanoparticles with fixed coordinates are explicitly present in the minimization process for the extraction of the primitive path network, and the "phantom particle limit" where nanoparticles are removed prior to the entanglement analysis. Simulation results indicate that the inclusion of nanoparticles into the polymer matrix does not significantly alter the polymer–polymer primitive path network. Instead, it enriches the nanocomposite system by nucleating additional topological constraints of polymer–particle origin.

I. Introduction

Nanoscale additives are capable of altering the structural, rheological, and mechanical properties of polymeric systems even at relatively low concentrations.[1] A fundamental understanding of blends of nanoparticles and polymers, often referred to as "polymer nanocomposites" (PNC), continues to be limited, particularly with regard to the mechanisms behind nanoparticle reinforcement. A better understanding of the dependence of reinforcement on additive properties could potentially lead to predictions of nanocomposite behavior as a function of particle size, shape, geometry and concentration, interfacial interactions, and, ultimately, to improve processing and preparation strategies. A number of recent reviews provide an overview of polymer-nanocomposite reinforcement.[2–6] Traditional models of filler reinforcement have primarily focused on the volume of the additive and its physical strength, without much concern for the nature of interactions between the filler and the polymer matrix.[7] In recent decades, the emergence of effective experimental preparation techniques for nanoinclusions has demonstrated that size and interaction strength can have pronounced effects on reinforcement.

Several new concepts have been put forward to interpret a variety of experimentally observed behaviors. The concept of an "interaction zone", for example, proposes that a reduced polymer mobility near the surface of particles increases the apparent size of the additive, thereby allowing small, high-surface-area particles to have a disproportionate influence on material properties with respect to their concentration.[8] The requisite polymer restructuring near nanoparticle surfaces has been confirmed by recent simulations,[9] which found evidence for the formation of a glassy layer surrounding the particles. Note that earlier simulations of polymer thin films had already anticipated that a layer of reduced mobility should arise in the vicinity of attractive surfaces.[10] More recent studies[11] have demonstrated strong reinforcement when glassy layers overlap, even below the percolation threshold. Alternatively, experimental studies of entangled PNCs during annealing below the glass transition temperature[12] have led to the proposition that particle aggregation and increased bridging between particles by polymer segments is responsible for the enhanced rheological properties of the composite. Note that simulations of short chains have suggested that a reduction in perpendicular mobility near filler surfaces correlates with long-lived polymer loops and bridges.[13] Such simulations, however, have traditionally been carried out with chains whose degree of polymerization is well below the entanglement molecular weight.

Several decades ago, Bueche proposed that particles may alter the underlying primitive path (PP) network of the polymer matrix by nucleating entanglements at the surface of the inclusions.[14] More recently, it has been suggested that the nonlinear viscoelastic properties of a PNC above the glass transition temperature are the result of how particle–polymer interfaces alter the underlying polymer matrix and the concomitant entanglement state of the system.[15] That view has been partly confirmed by simulations of rough spheres dispersed in entangled polymers, which have shown that nanoparticles lead to an increase in the observed plateau modulus, and correspondingly, the average number of entanglements.[16] Past simulations have focused on spherical inclusions; in this work, we examine whether particle shape also plays a role in the underlying entanglement network.

The mutual uncrossability of chains is central to any conceptual framework for understanding the rheological and

---

*Corresponding author. E-mail: depablo@engr.wisc.edu.

Published on Web 01/19/2011

mechanical behavior of entangled macromolecular systems. Doi and Edwards[17] introduced the concept of a PP as the shortest path between chain ends that is consistent with the restriction of chain uncrossability. Recently developed topological algorithms[18−21] have enabled the extraction of the PP network from simulations of polymer chains at various levels of detail. While original algorithms employed annealing and energy minimization techniques,[21] or lattice-based methods,[22] more recent approaches have relied on direct geometric−stochastic[19,20] algorithms for the minimization of the total contour length of the multiple disconnected primitive paths. Sukumaran et al.[18] demonstrated agreement between values for the plateau modulus derived from simulation-based calculations of entanglement molecular weight and those obtained from deformation experiments. They further showed that the contribution of the self-entanglements to the PP network was negligible for the simulated polymer systems. Tzoumanekas and Theodorou introduced the so-called "CReTA" algorithm[19] to examine the location of entanglements in a polymer melt. They found that the distribution of entanglements along a given polymer can be described by a stochastic point process whose distribution is the convolution of two exponential distributions. These authors proposed a corresponding master formula that was shown to have general applicability.[19,23,24] They also noted that beyond a short cutoff, the network structure could be described as an ideal gas of entanglements. Recent studies on fully flexible athermal polymer models,[23,25] employing the so-called "Z1" algorithm[20,26−28] for the extraction of PPs, have revealed a direct correspondence between interchain entanglements and intrachain knotting, and identified the scaling exponents for the dependence of entanglement statistics on volume fraction over the entire concentration range. The same algorithm had been used to obtain time-dependent quantities, such as the segment tube survival probability.[29] That probability allows for direct tests of the reptation theory and its refinements, including contour length fluctuations and constraint release.[30]

With few exceptions, simulation studies of entanglements have been restricted to pure polymer matrices. Riggleman et al.[16] used simulations and the CReTA algorithm to show that neutral spherical inclusions not only create new entanglements with the polymer matrix, but that polymer−polymer topological constraints are attracted to the particles during deformation. Richardson and Abrams[31] examined a rod-containing PNC during crazing, with rods being equally spaced and preferentially aligned perpendicular to the axis of deformation. They observed a decrease in the entanglements per chain during the course of multiaxial extension. More recently, Termonia examined polymer configurations in a fixed field of spherical particles using a lattice model,[32] and found that entanglement density increased with decreasing additive size.

The work presented here differs from past efforts in several respects. First, we simulate truly entangled, high molecular weight composites at equilibrium. Second, we focus on the effects of rod-like particles on the entanglement network, and we perform a systematic study of nanorod length. This is a pertinent choice, owing to the limited number of theoretical and computational studies available in the literature;[33] nanorod length is of particular fundamental interest because one can probe different length scales, and generate new knowledge that is currently missing from the theoretical nanocomposite literature. A critical examination of the nature of filler dispersion,[34−37] however, is beyond the scope of the current work. Additionally, examination of corresponding mechanical properties measurable via deformation of a PNC will be covered in another work.[38]

Our results indicate that, in the limit of "mobile" particles (see below for an explanation of this terminology), rod-like inclusions do not alter the underlying polymer PP network vis-à-vis that of the pure polymer. The effect of rod length on number of beads

between entanglements (N_e) is negligible in both limits, but is found to profoundly affect entanglement density. Deforming the composite induces the appearance of new particle−polymer entanglements, but does not increase the number of polymer−polymer entanglements.

II. Model and Methods

The composites considered here consist of long, fully flexible polymeric chains and semiflexible nanorods. A bead−spring representation is adopted for both the polymers and the rods. All polymer chains consist of $N = 500$ beads. Depending on the simulated system, the number of beads per nanorod ranges from 1 to 16, with beads being constrained in an almost linear (extended) conformation. Nonbonded interactions are governed by a 12−6 Lennard-Jones potential energy function of the form

$$U_{LJ}(r) = \begin{cases} 4\varepsilon\left[\left(\dfrac{\sigma}{r}\right)^{12} - \left(\dfrac{\sigma}{r}\right)^{6}\right], & r \le r_{in} \\ \sum_{j=0}^{4} C_j (r - r_{in})^j, & r_{in} < r \le r_c \\ 0, & r > r_c \end{cases} \quad (1)$$

where ε and σ are the Lennard-Jones parameters for energy and length, respectively, r is the distance between any two beads, r_c is a cutoff distance, r_{in} is the inner cutoff distance for a smoothed potential, and the C values are constants calculated so that the force and its first derivative go smoothly from the Lennard-Jones potential at the inner cutoff to zero at the outer cutoff distance. In this study, the inner and outer cutoff distances were set to 2.4σ and 2.5σ, respectively.

The value of ε is unity for polymer−polymer and particle−particle interactions, and is equal to 3 for polymer−particle interactions, thereby promoting mixing or dispersion of the rods within the polymer matrix. The bonded energy between two consecutive beads in the same chain/particle is given by a harmonic function of the form

$$U_{bond}(r) = k_r(r - r_o)^2 \quad (2)$$

where the spring-constant is set to $k_r = 10^3$ and $10^4 \times \varepsilon/\sigma^2$ for polymer bonds and nanorod bonds, respectively. The equilibrium bond length, r_o, is 1σ for polymer bonds and $2\sigma/3$ for the nanorods, thereby conferring to them a textured appearance. The rod-like character of the inclusions is enforced through a bending potential of the form

$$U_{bend}(r) = k_\theta(\theta - \theta_o)^2 \quad (3)$$

where θ is the bending angle formed by beads separated by two bonds, θ_o corresponds to the minimum-energy angle of 180°, and $k_\theta = 200\varepsilon \, \text{rad}^{-2}$.

Note that the diameter of both nanorod and polymer beads is the same, thereby allowing us to focus strictly on the effects of the aspect ratio of the inclusions, as opposed to behaviors that might arise from their large size vis-à-vis that of the chain monomer. Thus, our simulations correspond to PNCs containing monodisperse, short carbon nanotubes or nanowires in a polymeric material whose effective diameter is comparable with that of the inclusion.

As alluded to earlier, one of the main challenges associated with simulations of entangled PNC is that of sampling conformational space. Two issues must be addressed. First, the polymer itself must explore the configurational space made available to it within the field of topological constraints created by nanorods. Second, the nanorods must also explore the available phase space as efficiently as possible.

The first issue is handled primarily through implementation of connectivity-altering moves that juxtapose the ends of polymer chains.[39−42] Two forms of double-rebridging (DB) were used in this work; a configurational bias scheme along the lines of that proposed by Banaszak et al.,[40] as well as the Bondswap algorithm (BSA) of the LAMMPS[43] program. For DB, the first chain and a position on that chain were chosen at random. A Rosenbluth weight was then generated based on the distance between possible exchanged ends for each possible partner chain in the system, and then a partner was chosen randomly based on these weights. One bead was deleted from each chain, and 200 positions were attempted for the placement of new beads to connect the re-formed chains. The acceptance rate was approximately 0.05% for all systems.

For BSA simulations, a random list of all N atoms was created and then an N^2 search was performed for a pair of atoms such that all atoms involved in a potential bond-swap were within 1.2σ of each other. A swap was attempted and accepted according to Metropolis sampling criteria. The acceptance rate for BSA was between 4% and 6% for all systems. Because of the cutoff restriction, BSA acceptance rates do not differ considerably between PNC and pure polymer systems. As such, the rate of polymer relaxation is similar in all systems, even in the cases where the number of potentially viable swap sites differs between configurations.

Particle diffusion was ensured through implementation of a hybrid combination[44] of Monte Carlo and molecular dynamics moves, which enabled the smaller nanorod species to diffuse rapidly throughout the system. The time step employed for molecular dynamics (MD) was 0.001τ, using a velocity Verlet integration scheme. We use τ to denote Lennard-Jones time units such that $\tau = (m\sigma^2/\epsilon)^{1/2}$, where m is mass.

Each PNC system considered here consisted of 46 chains, for a total of 23 000 polymer beads. For comparison purposes, simulations were carried out on pure polymer systems of 81 chains having the same molecular length. For PNCs, rods of length 1, 4, 6, 8, 10, and 16 were considered at two different concentrations: 5.3 and 10 wt %. Because of the reduced bond length of $2/3\sigma$ for the nanorods, their aspect ratios were 1, 3, 4.33, 5.67, 7, and 11, respectively. For each combination of length and concentration, a set of 38 statistically uncorrelated trajectories were simulated. In the remainder of the text, nanocomposite systems are referred to by the size of their respective particles (e.g., 4-mer system).

The pure polymer and 4-mer, 8-mer, and 16-mer systems were constructed by growing chains to a number density of $0.5\sigma^{-3}$ around randomly dispersed nanorods using a traditional configurational bias insertion scheme.[45] Equilibration simulations of the nanocomposite systems, as well as subsequent production runs to produce independent configurations, were carried out at a reduced temperature of $1.75\epsilon/k_B$ and zero pressure, where k_B is the Boltzmann constant. These conditions are well above the glass transition temperature for the composites considered here,[38] the highest of which is $0.620\epsilon/k_B$ using a fast cooling rate. Each system then underwent cycles of 10^6 MD-step runs in the NPT-ensemble, and MC runs of 5 attempted double-rebridging moves per monomer bead, 25 attempted reptation moves per chain, and 100 attempted random displacements per bead. This process was continued until both the system volume and contour length of the primitive path (L_{pp}) stabilized. The procedure for calculation of the PP network and the entanglement molecular weight N_e is described later in the manuscript. The 1-mer, 6-mer, and 10-mer systems were constructed by shortening the rods of longer systems and randomly inserting new rods to reach the desired concentration. These systems were then subjected to a similar equilibration process. The final number densities obtained for these systems were 0.667 (pure polymer), 0.772 (1-mer), 0.797 (4-mer), 0.796 (6-mer), 0.792 (8-mer), and 0.770 (16-mer).

After the initial equilibration using DB, the generation of new independent states was achieved using LAMMPS with BSA moves enabled. It was verified that both the DB and BSA algorithms give
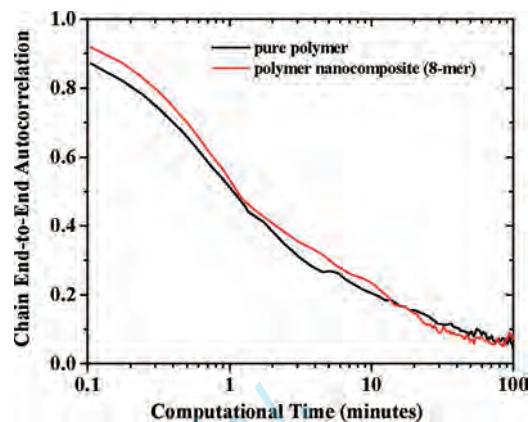
Figure 1. Orientational autocorrelation function of the end-to-end unit vector of polymer chains during MD simulation with bondswapping. PNC at 10.0 wt %.
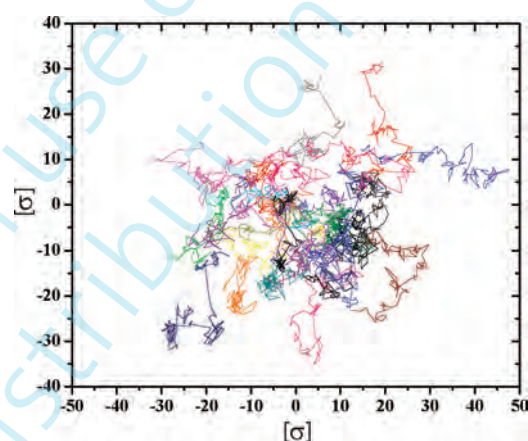
Figure 2. Trace in $x-y$ plane of typical 8-mer particle centers of mass during a LAMMPS run of 5000τ with bond-swapping enabled. Total box length is 31.88σ in each dimension.

comparable results for the average configurational properties of the polymer melts. Independent configurations were stored every 500,000 steps for subsequent extraction of the PP network and for calculation of entanglement statistics.

Figure 1 shows the average end-to-end vector autocorrelation function of the polymer chains for a pure polymer system and an 8-mer PNC. The long-range orientational relaxation of the polymer chains decays to 0.1 after approximately 1 h of computational time (on 4 processors using BSA), serving to demonstrate the efficiency of sampling achieved by MC bridging-based techniques and the validity and statistical relevance of the results presented in this work. After equilibration, all simulations were run long enough to ensure that the end-to-end autocorrelation function decayed multiple times. From the point of view of nanoparticle relaxation, a close examination of concurrent particle motion revealed random, diffusive behavior as demonstrated by the trace of nanorod centers of mass as projected on the xy-plane, shown in Figure 2. While the movement of longer rods is correlated with the directional vector along which the rod lies, a single long MD run allowed the rod-like particles to diffuse throughout the box and explore multiple orientations.

For completeness, multiple PP algorithms were used to generate the average molecular weight between entanglements, N_e. Note that while all PP algorithms are based on the same concept, their actual implementations can vary considerably, leading to subtle but important differences, particularly when considering composite systems. Sukumaran et al.[18] provided a method for constructing a PP through modified MD simulations.

That method fixes chain ends while slowly tightening polymer bonds. Thermal motion allows the chains to form a network of interconnected lines with negligible slippage around the ends of the polymer strands. While slippage has little impact on the calculation of entanglement statistics for a bulk system of 500-bead long chains (our early tests to choose a method showed no discrepancies for pure polymers), any slippage that occurs between a nanorod and a PP segment would add an unacceptable level of ambiguity to our analysis.

Alternatively, the CReTA scheme[19] involves a series of random aligning moves wherein chain beads are treated as hard spheres. In each move, the beads along a randomly selected segment of a polymer chain are rebuilt as a straight line with equidistant spacing. Any move that leads to interchain bead overlap or that moves a bead more than σ is rejected. This scheme prevents different chains from crossing, so long as the minimum distance between beads is kept sufficiently small. While individual straightening moves are fast, CReTA requires the addition of ever-larger numbers of beads to refine the PP at small length scales, thereby increasing the computational cost. Convergence is achieved once the maximum successful displacement (e.g., after 10 000 attempted trials) falls below a preset threshold.

The Z1 algorithm[20,26−28] constructs the entanglement network through a direct topological procedure, where each PP is treated as a connected path of infinitesimally thin, impenetrable and tensionless straight segments. Through an iterative and node-adaptive procedure, geometric operations monotonically minimize the total contour length of the multiple disconnected path simultaneously for all chains whose ends are held fixed in space. The multiple disconnected path is simply the sum of the contour lengths of the primitive paths. Convergence of the Z1 algorithm is achieved once the difference of the minimized total contour length between two successive iterations is smaller than a preset numerical tolerance.

In both the Z1 and CReTA methods, after successful minimization for each parent chain, a corresponding PP configuration is returned which is fully defined by the position vectors of the constituent internal kinks (the number of changes in PP direction, entanglement contacts) and their linear connectivity. Past studies have shown that, when applied to exactly the same bulk polymer configurations, the Z1 and CReTA algorithms provide comparable predictions for the statistics of the underlying PP network.[19,46,47] More details on the performance comparison of the existing methods for the extraction of the entanglement state of bulk polymer systems can be found in the literature.[26] In the interest of computational expediency, the Z1 method was chosen for the topological analysis presented in this work. Note, however, that we verified that CReTA and Z1 yield the same results for average contour length in our nanorod-polymer composite systems. Also note that in the present implementation of the Z1 method, which is based on geometric criteria, uncrossability between two chains can produce kinks either on both involved primitive paths (a "twin" event) or on just one of them (single occurrence).[27] In practice, nodes that do not change the direction of the PP and segments of vanishingly small length are disregarded in the calculation of entanglements.[48] As a result, the bond length and the bond angles of the resulting physical PP are non-zero. More details on the characterization of the PP network through the Z1 algorithm can be found in refs 26 and 27. Polymer−particle constraints were treated in the same manner as polymer−polymer constraints, and are based on the same geometrical criteria. To that end, the nanorod is represented as a cylindrical mesh composed of a large number of single-segment chains, whose lengths do not enter the calculation of L_{pp}. In the present version of the Z1 code, all nodes of the final PP are assigned to a particular contour position along the atomistic polymer, but information about the occurrence of binary and multiple entanglement events within the PP and their classification into polymer−polymer and polymer−particle contacts is not returned, i.e., there is no immediate distinction between polymer−particle and polymer−polymer contacts. Through this strategy, the contour length, L_{pp}, and the number of internal kinks, Z, of each PP become readily available. Once this information is extracted, the number of beads between entanglements, N_e, can be estimated according to

$$N_e^{\text{contact}} = \frac{(N-1)N}{Z(N-1)+N} \qquad (4)$$

where N is the number of beads of the parent chain. In the remainder of this manuscript we refer to eq 4 as the "contact" definition of N_e.[46,47] As an alternative which can also be applied when information about Z is not available from a PP analysis, Sukumaran et al.[18] proposed to consider the primitive paths as Gaussian chains, and to measure the mean squared end-to-end distance, R_{ee}^2, and the mean contour length L_{pp} of the PP. They then calculated N_e as

$$N_e^{\text{statistical}} = (N-1)\frac{R_{ee}^2}{L_{pp}^2} \qquad (5)$$

The latter equation will be referred to as the "statistical" interpretation of N_e. Contact and statistical expressions are identical to those based on "kinks" and "coils", respectively, as reported in the literature.[20,46,47,49,50] Refined N_e-estimators applicable down to weakly entangled systems $N \simeq N_e$ are also available.[49] Past independent studies[20,46,47] across different polymeric systems have reported significant differences between the predictions based on eqs 4 and 5. For melts in the density regime studied here, the statistical definition yields a value of N_e that is approximately twice that obtained from the contact calculation. The differences associated with these definitions have been thoroughly examined elsewhere[46] and are attributed to the non−Gaussian character of the PP.

In the case of PNCs we have been able to confirm that very similar deviations are observed in the values of N_e calculated by the two approaches. We prefer the contact definition because it entails a direct, assumption-free topological calculation of entanglements that remains valid for the case of nonequilibrium or constrained situations, where the configuration tensor embossing eq 5 becomes anisotropic. For completeness, however, results from both variants are presented here for PNCs at equilibrium.

It is worth mentioning that the number of beads between entanglements, N_e, is microscopically related to the length of the PP, denoted as L_{pp}, upon assuming that the PP represents a random walk with constant step length. Such an assumption is known to be somewhat crude, thus rendering L_{pp} the more fundamental quantity.[20,27,50]

The calculation of entanglements is particularly relevant in the context of the plateau modulus, G_e. The plateau modulus, which describes the constant-stress relaxation region of polymers in oscillatory shear experiments, is not directly accessible in simulations of highly entangled polymeric molecules. However, it is related to N_e by

$$G_e = \frac{4}{5}\frac{\rho k_B T}{N_e} \qquad (6)$$

where ρ is the density, k_B is Boltzmann's constant, and T is the temperature. Everaers et al.[21] have shown that simulations of N_e can be used to estimate G_e by eq 6, leading to good agreement with experiments.

An additional issue for the topological analysis of PNCs, not present in pure polymers, arises with the addition of particles. In one limit, these inclusions can be viewed as large, bulky, sticky objects that anchor to the polymers, thereby restricting motion and "tying" multiple polymer molecules together. This physical condition, which we refer to as "the frozen particle limit", is approximated by holding the nanorods fixed in space while applying the Z1 (or CreTA) algorithm to extract the PP. One can
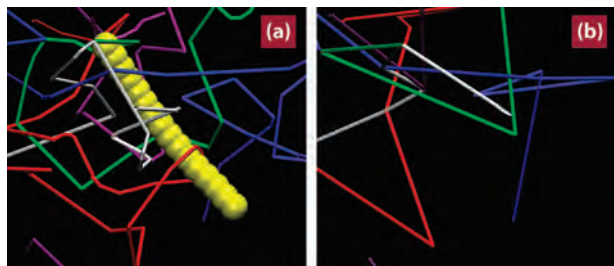
Figure 3. Primitive path network of polymer nanocomposites (a) in the frozen particle limit, where nanoinclusions are explicitly present and held fixed in space in the topological analysis, and (b) in the phantom particle limit, where nanorods are removed from the system before the extraction of the primitive paths. For clarity, only one nanorod and segments of three primitive paths are shown out of a 16-mer system at 10 wt %. Both images correspond to the same parent system configuration.

then determine all particle–chain entanglements directly, as illustrated in Figure 3a. At the other extreme, a particle can be viewed as relatively mobile, especially with respect to the sluggish motion of the chain molecules. In that limit, which we refer to as the "phantom particle limit", the particles are unable to restrict polymer motion on the time scales relevant to reptation dynamics. We approximate this latter limit, whose physical relevance rises with decreasing size of the inclusions, by removing the particles from the system prior to the PP analysis. In the phantom limit, particles only affect entanglement behavior in-so-far as they may alter the underlying polymer topology, as illustrated in Figure 3b. For completeness, we calculate the entanglement spacing in both the phantom and frozen particle limits; we expect the "true" value (and thus the effect of the nanoinclusions) to lie between the two. Shorter rods are more likely to behave as phantom particles, while the opposite stands as rod length increases.

The systems considered in this study are high-temperature melts, well above the glassy regime where rheological behavior is strongly related to the presence of entanglements. High-temperature conditions were chosen to facilitate equilibration. Past work with supercooled polymer melts[51] suggests that only a small, albeit systematic, decrease in N_e occurs when a system is cooled from the melt state to a glassy state. This is consistent with the physical viewpoint that glasses inherit their entanglement structure from the structure of the melt.

III. Melt Structure and Scaling

Our structural analysis of the PNC systems considered here begins with the calculation of the corresponding radial distribution functions, $g(r)$.

Figure 4 shows $g(r)$ for three of the nanocomposite systems: 1-mer, 8-mer, and 16-mer PNCs at 10 wt %. Note that figures are for systems quenched to a temperature of 0.3 (procedure described later) but are generally representative of the melt as well. Recall that the rods examined in this study each consist of spheres interconnected to each other. The $g(r)$ shown are for the interaction between individual sites in the rods, as opposed to the center of mass of the rods. For the monomeric particles, the polymer–polymer and polymer–particle $g(r)$ are nearly identical, except for the intensity of the first peak near contact. Both functions exhibit the oscillatory behavior that is characteristic of isotropic liquids. The first peak for the polymer–particle function is centered about $r = 2^{1/6}\sigma$. The polymer–polymer peak is slightly shifted to smaller r due to the inclusion of bonded polymer beads whose equilibrium bond length is 1σ. Examination of the particle–particle peak (which is inherently intermolecular for monomeric particles) reveals a slightly more complicated organization. Only a small peak exists near 1σ, indicating that particles are well dispersed and rarely come into contact. Instead, a strong peak is observed around 2σ, suggesting that particles distribute
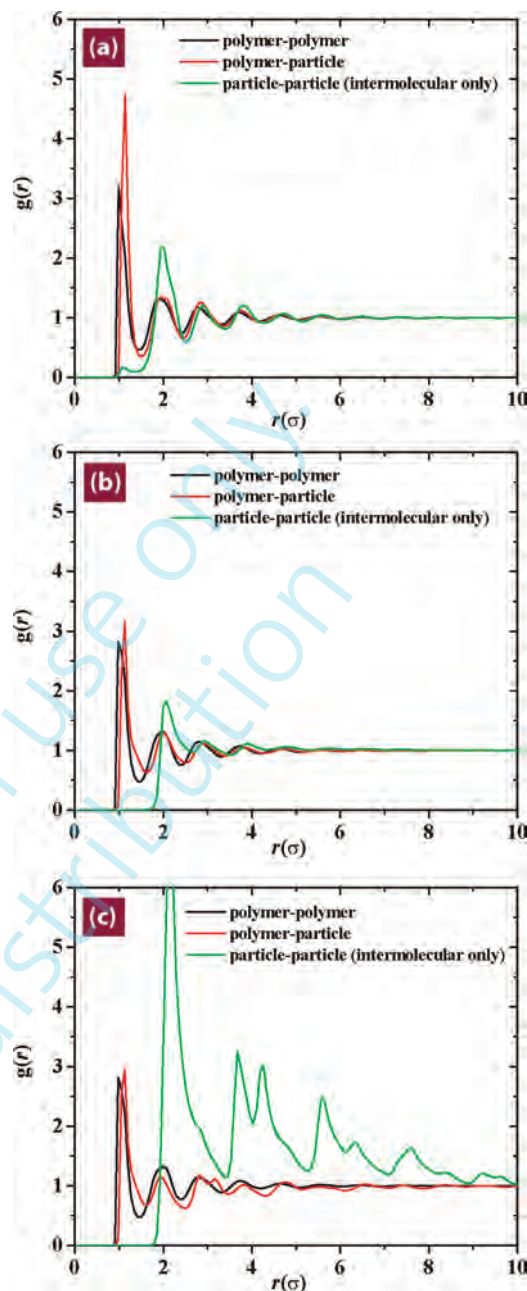

Figure 4. Radial distribution function curves of (a) 1-mer, (b) 8-mer, and (c) 16-mer PNC. Black denotes the polymer–polymer $g(r)$, including bonded beads, red denotes the polymer–particle $g(r)$, and green denotes the intermolecular particle–particle $g(r)$. All systems contain 10 wt % particles.

themselves throughout the system in such a way as to maintain a solvation layer of at least one polymer bead between them. The existence of this layer is confirmed by the high peak at contact for the particle–polymer $g(r)$. Intermolecular particle–particle neighbors are thus "pushed" into the second coordination shell. Aside from this short-ranged net repulsion, owing to preferential wetting of the particle surface by the polymer, monomeric particles do not influence each other.

The 8-mer system exhibits a number of features that are similar to those observed in the 1-mer composite. The polymer–polymer and polymer–particle $g(r)$ exhibit minor differences due to the steric constrains imposed by the rod architecture. The peak at 1σ in the intermolecular particle–particle $g(r)$ is no longer present, and the peak at 2σ is smaller. Just as the monomeric particles, the 8-mer rods are well dispersed in the polymer matrix and
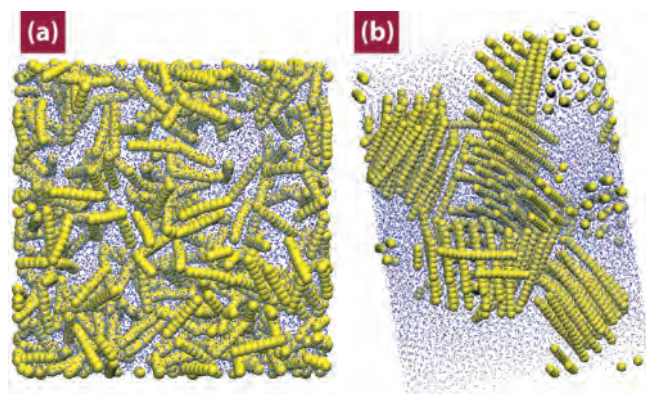
Figure 5. Visualization of representative 8-mer (a) and 16-mer (b) melt configurations. The nanorods are shown in yellow; polymers are shown in blue. Polymers are interwoven into particle clusters, most clearly seen in the top right of image (b). The radii of the polymer beads have been scaled down to improve clarity.
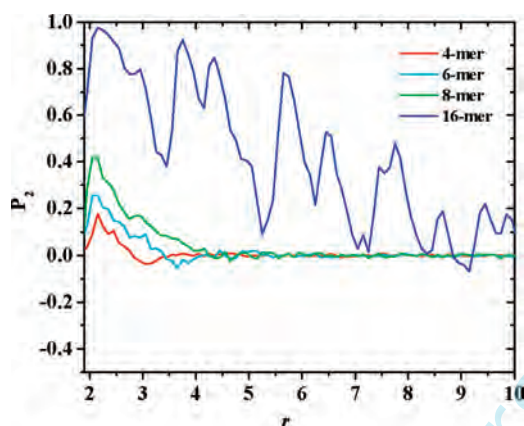

Figure 6. Local nanorod alignment as a function of center of mass separation (in units of σ). Alignment is defined as the second Legendre polynomial (P_2) of the dot product of the end-to-end vectors of a pair of rods. Averaged over a set of rod pairs, this value is −0.5 for perpendicular alignment, 1.0 for parallel alignment, and 0.0 for random alignment. Note that these results are shown only for rod separations after which the radial distribution of the center of mass of the rods first rises above 0.9. Results are shown for a 10 wt % nanorod weight fraction.

maintain a layer of polymer around them. This layer limits the nearest distance between pairs of rods, thereby making it less likely for a large number of beads in a rod to maintain a separation of exactly 2σ. The results for the 4-mer and 6-mer $g(r)$'s are qualitatively similar to those of the 8-mer.

Direct visualization of the 8-mer samples (Figure 5a) reveals that the rods are dispersed throughout the system with overall random orientation. Evaluation of local rod alignment as a function of distance between rods reveals very weak orientational correlations at distances smaller than the length of the corresponding nanorod (Figure 6). Only the 16-mer shows a high level of rod alignement, which persists over relatively large distances.

The polymer−polymer and polymer−particle $g(r)$ for the 16-mer are comparable to those for the smaller particle composites. However, the particle−particle $g(r)$ is considerably different. The magnitude of the peaks is much larger, the location of peaks no longer follows the other curves, and at radial distances beyond the range shown in the figure the intermolecular particle−particle $g(r)$ decays below unity. These factors arise because the 16-mer rods aggregate within the system, leading to a locally ordered structure. Figure 5b shows a representative configuration of the system, where it can be seen that nanorods form small bundles with a highly ordered local structure. Interestingly, the minimum
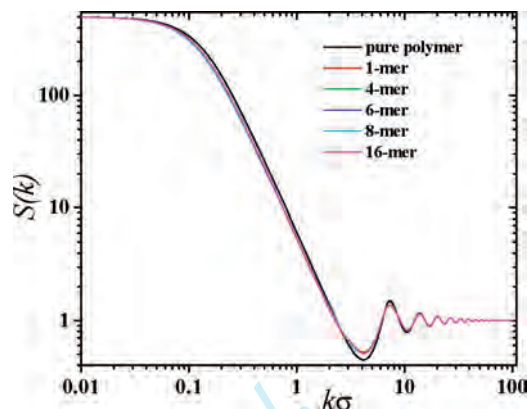
Figure 7. Static structure factor at 10 wt % filler.

distance between rods is still near 2σ, indicating that the resultant rod aggregates contain some polymer between the rods. Closer inspection of the polymer−particle $g(r)$ reveals minor changes from that of the 8-mer systems, most notably a small peak near 3.2σ. The polymer-mediated aggregation of otherwise repulsive small particles has been recently discussed by Hall and Schweizer,[34] who also noted this behavior in small cubes and disks.

A number of measures are used to examine the effect of particles on the structure of the polymer matrix. The static structure factor $S(k)$ is defined by

$$S(k) = \frac{1}{N}\left\langle \sum_i^N \sum_j^N \frac{\sin(\mathbf{k}\cdot\mathbf{r}_{ij})}{\mathbf{k}\cdot\mathbf{r}_{ij}} \right\rangle \tag{7}$$

where $\mathbf{k}$ is the scattering vector, k is its norm, N is the number of beads in a chain, i and j are indexes over all the beads in each chain, and $\mathbf{r}_{ij}$ is the distance vector between beads i and j. The brackets denote an average over chains and wave vector orientations. This functional form represents an alterative normalization over that generally considered in the literature.[52] By our normalization, $S(k)$ goes from a value equal to the number of beads in a chain, 500, at low k, to a value of unity at large k, due to self-interactions. Results are only shown for the polymer component of each system. As seen in Figure 7, for all the composites considered here, the structure factors of the polymer can be superimposed on top of each other, regardless of particle aspect ratio. Note, however, that $S(k)$ for the composites is different from that for the pure polymer. The most notable feature of the PNC curves is a slight kink near $k = 2\sigma^{-1}$, corresponding to length scales of approximately 3σ. For every system, the first peak of the static structure factor is at $k = 7.1\sigma^{-1}$. That first peak is often used to estimate the α relaxation in the system.

One can also extract a scaling exponent from the inverse of the static structure function's slope. This scaling exponent would be unity for a rigid rod, 0.5 for a random coil, and 0.588 for a self-avoiding random coil. For the smaller values of k ($0.135\sigma^{-1}$ to $0.625\sigma^{-1}$), corresponding to lengths of 10σ to 46σ between pairs of beads within the same chain, the exponent is between that of a random coil and a self-avoiding walk for all systems. For intermediate k ($0.625\sigma^{-1}$ to $1.85\sigma^{-1}$), giving lengths of 3.4σ to 10σ, the exponent approaches that of a random coil, but again there is little difference between the pure polymer and the nanocomposite systems. In contrast, for length scales between 2.3σ and 3.4σ, we see a dramatic difference. The exponent for the pure polymer melt corresponds to a random coil (scaling exponent is 0.488). But for the PNC systems, the scaling exponents are between 0.55 and 0.57, corresponding to a self-avoiding walk. The polymer chains solvate the particles and swell, consistent with the high level of local interactions suggested by the $g(r)$ (see Figure 4). Since the

nanorods are small and are well-solvated by the polymer, the overall structure of the macromolecules is only perturbed at these short length scales. Also note that the aggregated 16-mer systems do not exhibit significant differences from other PNCs. Similarly, results corresponding to 5.3 wt % nanorod loadings (not shown) can be superimposed onto the results shown in Figure 7.

The average mean-squared end-to-end distance, $\langle R_{ee}^2 \rangle$, of the polymer was also calculated for all systems. The standard error for all reported values of $\langle R_{ee}^2 \rangle$ was below $\pm 19\sigma^2$. For the pure polymer, $\langle R_{ee}^2 \rangle$ was $735\sigma^2$. The monomeric particle and 16-mer systems exhibit slightly higher values at $763\sigma^2$ and $761\sigma^2$ respectively, indicating a net swelling of the polymer molecules. The 4-mer, 6-mer, and 8-mer systems exhibit even higher values of $\langle R_{ee}^2 \rangle$, ranging from $789\sigma^2$ to $803\sigma^2$, even though $S(k)$ did not reveal any differences between these and the other nanocomposite systems. Values for the 5.3 wt % systems range from $778\sigma^2$ to 818σ, and are generally slightly larger than those observed for the 10 wt % nanorod loading.

Past studies[53] have argued that percolation is a necessary, but not sufficient, condition for the emergence of solid-like behavior in filled polymers. Here percolation is defined as the ability to create a continuous network of connected nanorods that spans the system (a simulation box) in any given dimension. As can be inferred from the radial distribution functions, each polymer bead has well-defined solvation shells. If contacts are defined as beads within a 1.5σ distance from each other, e.g., in each other's first solvation shell, then no system can percolate due to the layer of polymer between all additives. Note that the 8-mer rod system is just inside the semidilute regime, at a concentration above 9.43%, and the 16-mer is well inside that regime, at a concentration above 2.98%. Since the semidilute regime corresponds to the region of composition in which neighboring particles begin to pervade each other's volumes, it is a prerequisite for percolation. Alternatively, if one wishes to include the second solvation shell, and hence include that first layer of polymer as part of the particle (consistent with a zone-theory-like approach[8]), then all systems percolate. However, the latter definition requires that the vast majority of beads in the system be considered as part of the nanorod particles.

It is of particular interest to examine the nature of particle–polymer bridges, and determine how they vary with rod length. Literature studies[12,13,54] have suggested that an underlying polymer–particle network, consisting of particles connected by polymer bridges, is responsible for nanoparticle-induced strengthening. In this work, a bridge is defined as a subset of sequential polymer beads along the same chain such that the first bead is within 1.5σ of a nanorod, the last bead is within 1.5σ of a different particle, and no intermediate bead is in contact with any rod. The cutoff distance is taken to be the value of the first dip in the rod–polymer radial distribution function. Under this definition two types of bridges can exist, namely single-bead and multibead. A single-bead bridge consists of a polymer bead in contact with two different rods. Single-bead bridges constitute a significant fraction of the bridges observed in our systems. Multibead bridges are all bridges that consist of more than 1 bead.

Figure 8 shows the number of bridges per nanorod as a function of rod length and concentration, with single and multibead contacts shown separately. The number of bridges is normalized with respect to the number of nanorods (as opposed to nanorod beads). It can be seen that the total number of bridges, which is the summation of the two contributions, increases strongly with rod length at both concentrations. However, when single-bead and multibead bridges are considered separately two trends emerge. First, for 8-mers and larger rods, the number of multibead bridges per particle does not change with aspect ratio, while the number of single-bead bridges increases markedly. Single-bead bridges, by definition, require the bridged rods to be in close
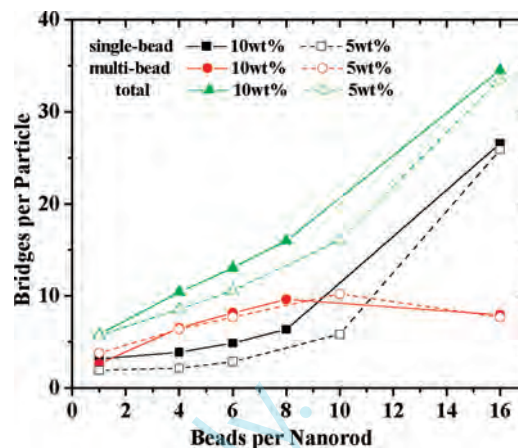
Figure 8. Normalized number of polymer bridges that each nanorod is connected to. The number of beads per nanorod is approximately equal to the aspect ratio. Black (squares), red (circles), and green (triangle) lines denote single-bead, multibead, and total bridges, respectively. Solid lines with filled shapes correspond to 10 wt % loading and dotted lines with hollow shapes correspond to 5% loading. Error bars in these calculations are smaller than the size of the symbols.

proximity. Specifically, in the present analysis the maximum distance that can be bridged between two nanorods by a single chain beads is 3σ. The sharp increase in the single-bead bridge population comes from extensive trapping of polymer segments between particle beads and extensive aggregation (and thus ordering) of 16-mer nanorods. Within the model considered here, the presence of single-bead bridges is correlated to clustering.

While the number of single-bead bridges increases with concentration (except for 16-mers), the number of multibead bridges per particle is nearly independent of concentration, within the range considered here. There is an almost perfect overlap between the two red curves (both marked by circles) shown in Figure 8. At low concentrations, one would expect that inserting a new particle should provide more possible connections for each old particle to bridge to, affecting number of bridges in a nonlinear way. Over the concentration range considered here, our results suggest that the number of multibead bridges per particle has reached a saturation concentration. This saturation effect does not apply to single-bead bridges, other than in the 16-mer system.

IV. Entanglements

A. Quiescent State. Our pure polymer at a temperature of $1.75\epsilon/k_B$ and zero pressure has a lower number density, $0.667\sigma^{-3}$, than that slightly above the glass transition temperature, a regime that has been studied extensively with Lennard-Jones polymers. To determine the role of density on entanglements, we performed additional simulations of the pure polymer at a constant number density of 0.975, comparable to that employed in past studies of dense melts. The entanglement "length" N_e at high density is 43.6 ± 1.4 and it is 56.0 ± 3.5 at the lower density (for the contact definition). These values become 75.5 ± 6.0 and 106.7 ± 14.1, respectively, for the statistical definition. These results are consistent with the scaling of N_e with density for model fully flexible athermal polymers reported in the literature.[23] Also note that the result obtained here for the pure polymer at high density in the statistical limit is in good agreement with available literature data.[18]

For the PNC systems, N_e was determined as a function of rod length in both the phantom- and frozen-particle limits, using both the statistical and contact definitions. The results are shown in Figure 9. There is excellent qualitative agreement between the contact and statistical definitions, with
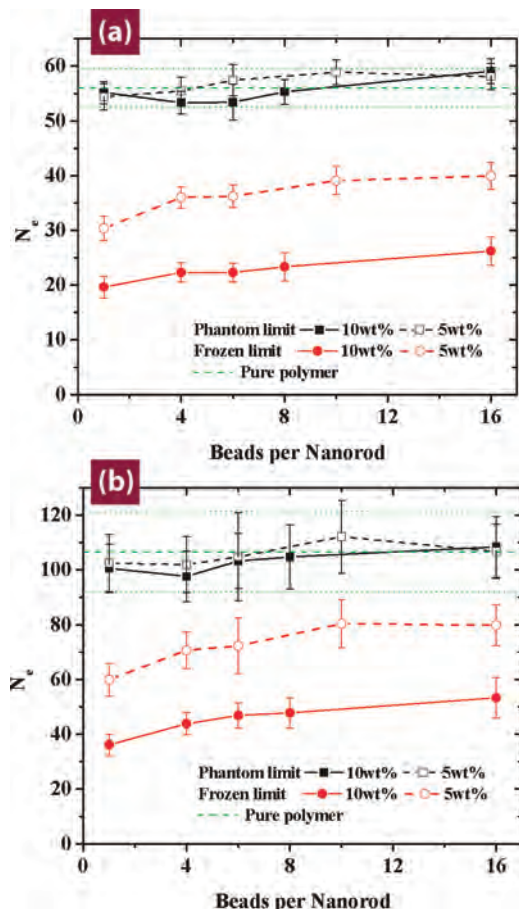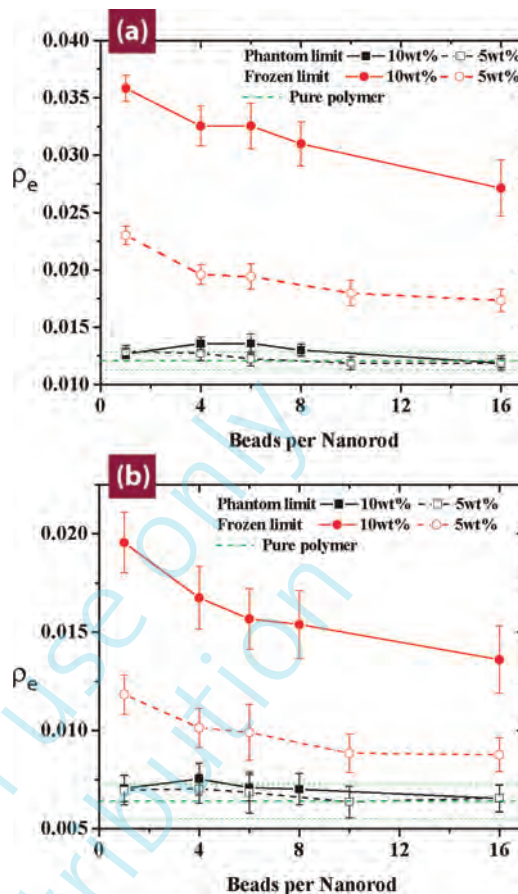
Figure 9. Number of beads between entanglements, N_e, as a function of rod length in nanocomposite systems under the contact definition (a) and the statistical definition (b), both evaluated via the Z1 algorithm. The black lines denote the frozen particle limit (with particle) and the red lines denote the phantom particle limit (removed particle). Filled symbols are used for systems at 10 wt % and open symbols for systems at 5.3 wt %. The green line denotes results for the pure polymer. Error bars correspond to one standard deviation.


Figure 10. Entanglement density ρ_e, as a function of rod length in nanocomposite systems under the contact definition (a) and statistical definition (b). The black lines denote the frozen particle limit (with particle) and the red lines denote the phantom particle limit (removed particle). Filled symbols are used for systems at 10 wt % and open symbols for systems at 5.3 wt %. The green line denotes results for the pure polymer. These results were generated using the melt density corresponding to the temperature at which the N_e calculations were performed.

regards to the dependence of N_e on the length of the nanoparticles. However, as expected, the absolute values for the contact and statistical definitions differ by a constant factor of 1.91 for pure polymer, 2.00 for 5 wt % PNC, and 1.86 for 10 wt % PNC. The ratio found here for the pure polymer case falls within the range of published data for various atomistic and coarse−grained polymer systems.[20,46,47,49]

In the frozen particle limit, shown by the black curves, where nanoparticles are considered explicitly in the topological analysis, N_e exhibits a significant decrease from its pure polymer value. In the phantom particle limit, shown by the red curves, only small deviations from the value of the pure polymer are observed, and these lie within the statistical uncertainty of our N_e estimates. That is, when the particles are not included explicitly in the PP analysis, our results for N_e are the same as those for the pure polymer. This implies that the inclusion of nanoparticles does not alter the underlying PP mesh of the polymer itself. A higher number of entanglements is a direct result of contacts with the nanorods. For nanocomposites, changes in mechanical properties associated with entanglements should therefore be viewed as a result of direct interaction mechanisms (direct contacts or entanglements) between polymer and inclusions, and not the result of subtle network alterations to the underlying polymer−polymer topological constraints. Monomeric particles

show the most pronounced deviations. Differences in N_e among the various nonspherical inclusions are small.

One can count the actual number of polymer−particle entanglements, and normalize that count with the length of the particles. That analysis reveals that the number of entanglements per unit length (physical length, not beads per nanorod) of inclusion is essentially constant across all additive lengths. In the contact limit, this value is 0.30 ± 0.03 for the 10 wt % systems and 0.23 ± 0.03 for 5.3 wt % systems. Differences in density only account for about 0.01 entanglements per unit length of the change. That is, the number of entanglements per particle length is higher for larger concentrations over the range of concentrations considered here. Simulations of systems containing only an individual nanorod (results not shown) yield an entanglement density per unit length equal to that observed for the 5.3 wt % systems. The entanglement increase therefore arises for concentrations between 5 and 10 wt %, and at higher concentrations it will be limited by the solubility of the rods in the polymer.

For spherical nanoparticles, the definition of entanglements requires that the smooth edges of the inclusions do not allow the chains to slip by. A monotonic decrease of the PP length is an integral part of the quasi−topological approach, because *all* entanglements could otherwise be generally removed upon slipping over chain ends in concert with a
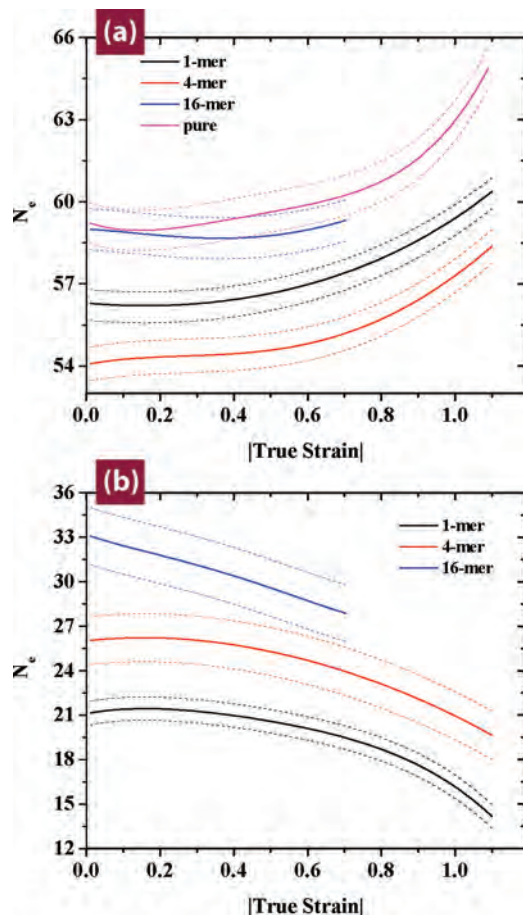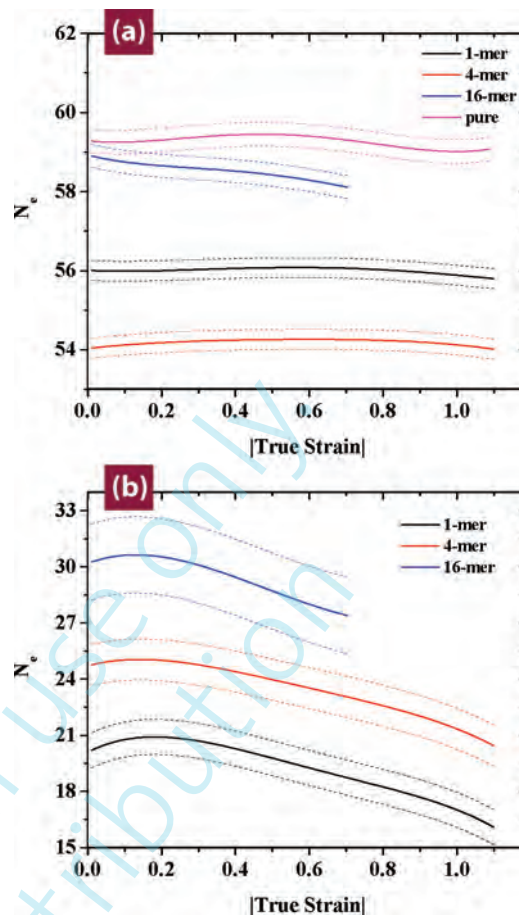
Figure 11. Changes to N_e during extension under the contact definition in the phantom (a) and frozen (b) particle limits at 10 wt % filler. Dashed lines denote the range on fluctuations of average across all samples.


Figure 12. Changes to N_e during compression under the contact definition in the phantom (a) and frozen (b) particle limits at 10 wt % filler. Dashed lines denote the range on fluctuations of average across all samples.

temporary increase of the PP contour length. While entanglements are thus consistently defined and detected, for such a system the frozen limit is unlikely to provide a realistic representation of the physics of truly small inclusions. The error bars for the monomeric particle systems are small due to the reproducibility of the measurement, but the actual relevance of such entanglements is questionable. For spherical particles a "rough" nanoparticle model is more appropriate, as presented by Riggleman et al.[16]

Note that all the systems considered here were simulated at the same pressure. The N_e results in the phantom limit are the same for the PNCs and the pure polymer, despite the different densities observed in these systems. At zero pressure, however, the pure polymer exhibits a number density of $0.667\sigma^{-3}$ that is significantly lower than that of the PNCs, whose number density is in the range from $0.770\sigma^{-3}$ to $0.797\sigma^{-3}$,[38] depending on rod length. On the basis of known scaling relations for entanglement molecular weight with density in athermal polymers,[23] we anticipate that the pure polymer at the density of the PNC (0.770) would exhibit $N_e \approx$ 50 (contact value) or $\approx$96 (statistical value). When compared at the same density, the phantom and pure polymer results for N_e continue to be the same within the statistical uncertainty of our simulations, although slight differences begin to appear between the pure polymer and the PNC begin to appear in the contact limit.

The molecular weight between entanglements is related to the plateau modulus of the material, as noted in eq 6. Since, the density of each PNC is different, one can analyze the data

in terms of entanglement density ρ_e, defined as bead number density divided by N_e. The results for the dependence of entanglement density on rod length in both limits are shown in Figure 10, with graph colors (and symbols) being fully consistent with the previous N_e figures. A detailed theoretical study of the effect of density and polymer stiffness on entanglement densities for pure polymers is available in the literature.[55]

As discussed above, the statistical and contact definitions show the same trends, not withstanding the quantitative differences. The contact definition predicts larger enhancements of the plateau modulus than the statistical definition. In the frozen particle limit there is a clear decrease in entanglement density with increasing rod length. Recall that the true value of N_e and entanglement density lies somewhere between the phantom and frozen particle limits, and where it falls between those limits is likely a function of particle length. As such, we expect our 16-mer system to begin approaching the frozen limit, which would suggest a nearly 2-fold increase in plateau modulus over that of the pure polymer for systems containing equilibrated long rods.

B. Deformed State. It is of interest to examine the instantaneous values of N_e during deformation, since our calculations are based on an analysis of configurations and not on a dynamic measurement. To obtain these values, each system was rapidly cooled to a temperature of $0.3\epsilon/k_B$ over 900τ, aged for 1000τ at constant volume, and deformed at a constant elongational strain rate of $0.0044\tau^{-1}$ until a final true strain of 1.09.
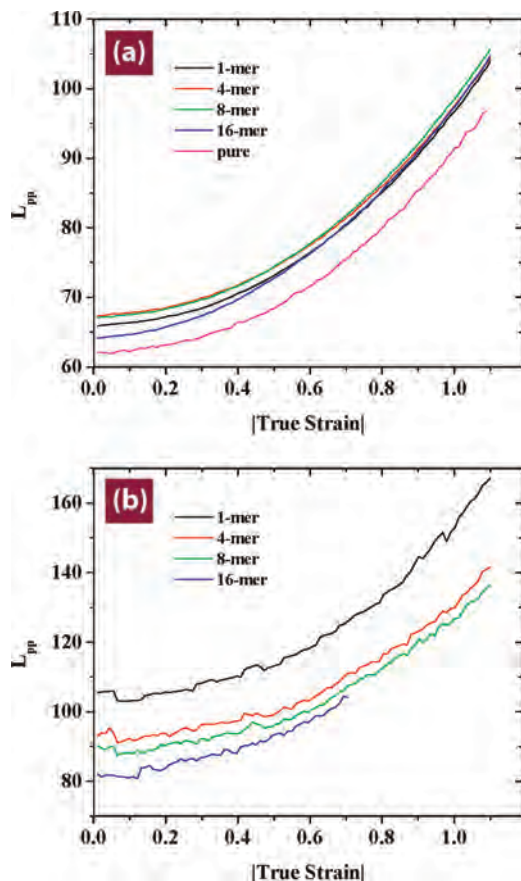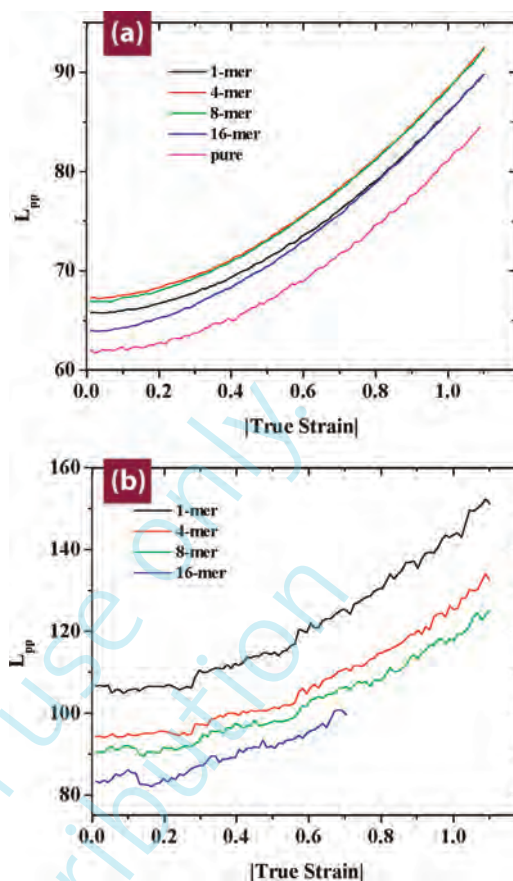
Figure 13. Changes to L_{pp} (in units of σ) during extension under the contact definition in the phantom (a) and frozen (b) particle limits at 10 wt % filler.

Figure 14. Changes to L_{pp} during compression under the contact definition in the phantom (a) and frozen (b) particle limits at 10 wt % filler.

Under these conditions, the density remains nearly constant. Results for 16-mer rods are truncated well before the smallest box—dimensions reach the length of the rod. Note that the validity of the random—coil assumption of the PP is invalid during deformation, and therefore only the results from the contact definition are reported in what follows.

Full details of this deformation procedure and corresponding mechanical analysis can be found elsewhere.[38] For completeness, we only note here that the elastic responses of all PNCs are comparable, but markedly stronger than that of the pure polymer. Yield occurs at strains around 0.05. As will be seen shortly, virtually no change in N_e occurs over the elastic regime. After yield, however, N_e changes considerably. Post-yield, PNCs exhibit a larger hardening modulus with increasing rod length during tensile deformation, but show no such trend during compressive deformation.

Figures 11 and 12 show results for the evolution of N_e as a function of strain under extension and compression, respectively. For clarity, for each curve a fourth-order polynomial fit of the raw data is shown; the dotted lines serve to represent the statistical error associated with each curve.

We first examine the tensile deformation of the PNCs in the phantom limit. Figure 11a shows a weak but systematic increase in N_e, with the rate of the increase being larger at higher strains. The pure polymer behaves similarly. Note that the pure polymer results here are the average of only three configurations, as compared to 38 for the nanocomposites, thus accounting for their larger fluctuations. The trend in N_e during deformation is consistent with the view that entanglements are able to slip free of each other as the polymeric material is uniaxially stretched[56] (this reference also

discusses qualitative differences that arise in shearing flows). However, in the frozen particle limit, Figure 11b, a more complex behavior emerges. At low strain rates, N_e increases slightly after the yield point,[38] after which the system becomes more entangled, as seen by the decrease in N_e.

As mentioned earlier, at equilibrium the entanglements in the phantom limit are representative of the polymer—polymer entanglements. The additional entanglements that arise in the frozen limit correspond to direct polymer—particle interactions. Assuming this observation remains valid during deformation, beyond the yield point we observe a simultaneous decrease in polymer—polymer (phantom limit) entanglements and an increase in polymer—particle (frozen limit) entanglements. As seen in Figure 11, this qualitative behavior is not affected by the rod length.

Examination of N_e during compression shows a similar distinction between polymer—polymer and polymer—particle entanglements, as seen in Figure 12. In compression, N_e is virtually unchanged in the phantom limit, but decreases in the frozen limit. Results using the CReTA algorithm (not shown) provide the same trends for the evolution of N_e with strain under uniaxial deformation.

The increase in polymer—particle entanglements observed under both modes of deformation is consistent with the clustering of entanglements about the particle observed by Riggleman et al.[16] Richardson and Abrams[31] showed the opposite trend in N_e, with the number of entanglements per chain decreasing during deformation in simulations near the frozen limit. However, they used a different PP algorithm, their rods were prealigned perpendicular to the direction of deformation, and they worked across much higher strain rates, making comparisons between their results and ours difficult.

While not directly relevant to the entanglement state once the system is perturbed from equilibrium, it remains possible to characterize the PNC by the L_{pp} extracted during PP analysis. This parameter-free measure of the system is of particular relevance, as the physical information on the PP is reflected by the shape and total contour length of the path. Figures 13 and 14 show raw L_{pp} averages for all systems. In all cases, L_{pp} increases with deformation in a similar fashion. The frozen limit results are somewhat noisier, owing to the fluctuations in number of particle−polymer contacts, with higher L_{pp} values due to the additional topological constraints created by the inclusions. There is little difference between compression and extension results.

V. Conclusion

The fact that nanoparticles reinforce polymers is well-established, but fundamental disagreements remain about the nature and the origins of this strengthening. To examine possible mechanisms, we first analyzed the presence of polymer bridges between inclusions. We found a notable increase in bridges formed with increasing rod length, consistent with the large surface area of those species. However, when we categorized those bridges based upon their length, we found that single-bead bridges accounted for all of the increase in number of bridges per particle for the longest rods. These single-bead bridges are indicative of shorter-length-scale interactions, and not the extended network of bridges as normally invoked to explain nanoparticle reinforcement. Given the extremely small diameter of our particles, it is not expected that single-bead bridges contributed notably in previous works.

A second explanation of reinforcement focuses on how nanoparticles alter the underlying PP network. Here, we performed extensive topological analysis on equilibrated rod-containing PNC to extract the entanglement state. In the frozen particle limit, particles were treated as immobile objects, while in the phantom particle limit they were treated as too mobile to restrict reptative movement and were removed prior to PP analysis. These limits represent the logical extremes of particle behavior, thus ensuring the true systems' values are bounded by their results. As such, we have provided a basis for evaluation of geometrical entanglements in a nanocomposite system. Where the true value lies within these bounds is a matter of how correlated particle−polymer motion is on the time scales of reptation, which itself is suspected to be a function of particle geometry.

The PP analysis revealed two unexpected results. First, it was observed that the entanglement molecular weight of the polymer is recovered from the nanocomposite in the phantom particle limit. This implies that inclusions do not alter the underlying polymer network, rather, all particle reinforcement should be attributable to direct interactions. Second, we found that N_e demonstrated complex behavior during rapid deformation, in the frozen particle limit. Specifically there is a decrease (extension) or no change (compression) in the number of polymer−polymer entanglements as observed via the phantom particle limit, but the number of polymer−particle entanglements increases in both cases. This implies that nanocomposites attract new entanglements during deformations without preventing the natural release of polymer−polymer entanglements.

What we cannot comment on from a static PP analysis is the disentanglement time associated with those constraints. It remains unclear whether entanglements resulting from particles are easier or harder to disentangle than those that occur between chains. Furthermore, it is possible that as particles impart generally slower dynamics into chain segments, they reduce the polymer's ability to reptate freely from chain−chain entanglements as well. Further dynamical evaluation of these systems will be performed in a future work.

References and Notes

(1) Winey, K. I.; Vaia, R. A. Polymer nanocomposites. *MRS Bull.* **2007**, *32*, 5.

(2) Akcora, P.; Kumar, S. K.; Moll, J.; Lewis, S.; Schadler, L. S.; Li, Y.; Benicewicz, B. C.; Sandy, A.; Narayanan, S.; Illavsky, J.; Thiyagarajan, P.; Colby, R. H.; Douglas, J. F. "Gel-like" mechanical reinforcement in polymer nanocomposite melts. *Macromolecules* **2010**, *42*, 1003–1010.

(3) Komarneni, S. Nanocomposites. *J. Mater. Chem.* **1992**, *2*, 1219–1230.

(4) Kamel, S. Nanotechnology and its applications in lignocellulosic composites, A mini review. *eXPRESS Polym. Lett* **2007**, *1*, 546–575.

(5) Huang, Z. M.; Zhang, Y. Z.; Kotaki, M.; Ramakrishna, S. A review on polymer nanofibers by electrospinning and their applications in nanocomposites. *Compos. Sci. Technol.* **2003**, *3*, 2223–2253.

(6) Gangopadhyay, R.; De, A. Conducting polymer nanocomposites: a brief overview. *Chem. Mater.* **2000**, *12*, 608–622.

(7) Halpin, J. C.; Kardos, J. L. The Halpin−Tsai equations: a review. *Polym. Eng. Sci.* **1976**, *16*, 344–352.

(8) Berriot, J.; Montes, H.; Lequeux, F.; Long, D.; Sotta, P. Evidence for the shift of the glass transition near the particles in silica-filled elastomers. *Macromolecules* **2002**, *35*, 9756–9762.

(9) Papakonstantopoulos, G. J.; Doxastakis, M.; Nealey, P. F.; Barrat, J. L.; de Pablo, J. J. Calculation of local mechanical properties of filled polymers. *Phys. Rev. E* **2007**, *75*, 031803.

(10) Torres, J. A.; Nealey, P. F.; de Pablo, J. J. Molecular simulation of ultrathin polymeric films near the glass transition. *Phys. Rev. Lett.* **2000**, *85*, 3221–3224.

(11) Merabia, S.; Sotta, P.; Long, D. R. A Microscopic Model for the Reinforcement and the Nonlinear Behavior of Filled Elastomers and Thermoplastic Elastomers (Payne and Mullins Effects). *Macromolecules* **2008**, *41*, 8252–8266.

(12) Zhang, Q.; Archer, L. A. Poly (ethylene oxide)/silica nanocomposites: structure and rheology. *Langmuir* **2002**, *18*, 10435–10442.

(13) Vacatello, M. Monte Carlo simulations of polymer melts filled with solid nanoparticles. *Macromolecules* **2001**, *34*, 1946–1952.

(14) Bueche, F.. *Reinforcement of elastomers*; Interscience: New York, 1965.

(15) Sternstein, S. S.; Zhu, A. J. Reinforcement mechanism of nano-filled polymer melts as elucidated by nonlinear viscoelastic behavior. *Macromolecules* **2002**, *35*, 7262–7273.

(16) Riggleman, R. A.; Toepperwein, G. N.; Papakonstantopoulos, G. J.; Barrat, J. L.; de Pablo, J. J. Entanglement network in nanoparticle reinforced polymers. *J. Chem. Phys.* **2009**, *130*, 244903.

(17) Doi, M.; Edwards, S. F.. *The Theory of Polymer Dynamics*. Oxford University Press: Oxford, U.K., 1986.

(18) Sukumaran, S. K.; Grest, G. S.; Kremer, K.; Everaers, R. Identifying the primitive path mesh in entangled polymer liquids. *J. Polym. Sci., Part B* **2005**, *43*, 917–933.

(19) Tzoumanekas, C.; Theodorou, D. N. Topological Analysis of Linear Polymer Melts. *Macromolecules* **2006**, *39*, 4592–4604.

(20) Kröger, M. Shortest multiple disconnected path for the analysis of entanglements in two-and three-dimensional polymeric systems. *Comput. Phys. Commun.* **2005**, *168*, 209–232.

(21) Everaers, R.; Sukumaran, S. K.; Grest, G. S.; Svaneborg, C.; Sivasubramanian, A.; Kremer, K. Rheology and microscopic topology of entangled polymeric liquids. *Science* **2004**, *303*, 823.

(22) Shanbhag, S.; Larson, R. G. Chain retraction potential in a fixed entanglement network. *Phys. Rev. Lett.* **2005**, *94*, 076001.

(23) Foteinopoulou, K.; Karayiannis, N. C.; Laso, M.; Kröger, M.; Mansfield, M. L. Universal scaling, entanglements, and knots of model chain molecules. *Phys. Rev. Lett.* **2008**, *101*, 265702.

(24) Spyriouni, T.; Tzoumanekas, C.; Theodorou, D. N.; Müller-Plathe, F.; Milano, G. Coarse-grained and reverse-mapped united-atom simulations of long-chain atactic polystyrene melts: Structure, thermodynamic properties, chain conformation, and entanglements. *Macromolecules* **2007**, *40*, 3876–3885.

(25) Laso, M.; Karayiannis, N. C.; Foteinopoulou, K.; Mansfield, M. L.; Kröger, M. Random packing of model polymers: local structure, topological hindrance and universal scaling. *Soft Matter* **2009**, *5*, 1762–1770.

(26) Shanbhag, S.; Kröger, M. Primitive path networks generated by annealing and geometrical methods: Insights into differences. *Macromolecules* **2007**, *40*, 2897–2903.

(27) Karayiannis, N. C.; Kröger, M. Combined molecular algorithms for the generation, equilibration and topological analysis of entangled polymers: Methodology and performance. *Int. J. Mol. Sci.* **2009**, *10*, 5054.

(28) The Z1 application is permanently available online at http://www.complexfluids.ethz.ch/Z1.

(29) Stephanou, P. S.; Baig, C.; Tsolou, G.; Mavrantzas, V. G.; Kröger, M. Quantifying chain reptation in entangled polymer melts: Topological and dynamical mapping of atomistic simulation results onto the tube model. *J. Chem. Phys.* **2010**, *132*, 124904.

(30) McLeish, T. C. B. Tube theory of entangled polymer dynamics. *Adv. Phys.* **2002**, *51*, 1379.

(31) Richardson, D. G.; Abrams, C. F. The effects of nanotube fillers on craze formation in simulated glassy polymers under tensile load. *Mol. Simul.* **2007**, *4*, 421–427.

(32) Termonia, Y. Chain Confinement in Polymer Nanocomposites and Its Effect on Polymer Bulk Properties. *J. Polym. Sci., Part B* **2010**, *48*, 687–692.

(33) Ganesan, V. Some issues in polymer nanocomposites: Theoretical and modeling opportunities for polymer physics. *J. Polym.Sci. B* **2008**, *46*, 2666–2671.

(34) Hall, L. M.; Schweizer, K. S. Structure, scattering patterns and phase behavior of polymer nanocompsites with nonspherical fillers. *Soft Matter* **2010**, *6*, 1015–1025.

(35) Kim, K.; Utracki, L. A.; Kamal, M. R. Numerical simulation of polymer nanocomposites using self-consistent meanfield model. *J. Chem. Phys.* **2004**, *121*, 10766.

(36) Zhao, L.; Li, Y. G.; Zhong, C.; Mi, J. Structure and effective interactions in polymer nanocomposite melts: An integral equation theory study. *J. Chem. Phys.* **2006**, *124*, 144913.

(37) Pütz, K.; Krishnamoorti, R.; Green, P. F. The role of interfacial interactions in the dynamic mechanical response of functionalized SWNT−PS nanocomposites. *Polymer* **2007**, *48*, 3540–3545.

(38) Toepperwein, G. N.; Riggleman, R. A.; de Pablo, J. J. Dynamics and Deformation Responce of Rod-Containing Polymer Nanocomposites. Manuscript in preparation, **2011**.

(39) Karayiannis, N. C.; Giannousaki, A. E.; Mavrantzas, V. G.; Theodorou, D. N. Atomistic Monte Carlo simulation of strictly monodisperse long polyethylene melts through a generalized chain bridging algorithm. *J. Chem. Phys.* **2002**, *117*, 5465.

(40) Banaszak, B. J.; de Pablo, J. J. A new double-rebridging technique for linear polyethylene. *J. Chem. Phys.* **2003**, *119*, 2456.

(41) Papakonstantopoulos, G. J.; Yoshimoto, K.; Doxastakis, M.; Nealey, P. F.; de Pablo, J. J. Local mechanical properties of polymeric nanocomposites. *Phys. Rev. E* **2005**, *72*, 031801.

(42) Sides, S. W.; Grest, G. S.; Stevens, M. J.; Plimpton, S. J. Effect of end-tethered polymers on surface adhesion of glassypolymers. *J. Polym. Sci., Part B* **2004**, *42*, 199–208.

(43) Plimpton, S. Fast parallel algorithms for short-range molecular dynamics. *J. Comput. Phys.* **1995**, *117*, 1–19.

(44) Gromov, D. G.; De Pablo, J. J. Structure of binary polymer blends: Multiple time step hybrid Monte Carlo simulations and self-consistent integral-equation theory. *J. Chem. Phys.* **1995**, *103*, 8247.

(45) de Pablo, J. J.; Laso, M.; Suter, U. W. Simulation of polyethylene above and below the melting point. *J. Chem. Phys.* **1992**, *96*, 2395.

(46) Foteinopoulou, K.; Karayiannis, N. C.; Mavrantzas, V. G.; Kröger, M. Primitive path identification and entanglement statistics in polymer melts: Results from direct topological analysis on atomistic polyethylene models. *Macromolecules* **2006**, *39*, 4207–4216.

(47) Kamio, K.; Moorthi, K.; Theodorou, D. N. Coarse grained end bridging Monte Carlo simulations of poly (ethylene terephthalate) melt. *Macromolecules* **2007**, *40*, 710–722.

(48) Foteinopoulou, K.; Karayiannis, N. C.; Laso, M.; Kröger, M. Structure, Dimensions, and Entanglement Statistics of Long Linear Polyethylene Chains. *J. Phys. Chem. B* **2009**, *113*, 442–455.

(49) Hoy, R. S.; Foteinopoulou, K.; Kröger, M. Topological analysis of polymeric melts: Chain-length effects and fastconverging estimators for entanglement length. *Phys. Rev. E* **2009**, *80*, 031803.

(50) Tzoumanekas, C.; Lahmar, F.; Rousseau, B.; Theodorou, D. N. Onset of Entanglements Revisited. Topological Analysis. *Macromolecules* **2009**, *42*, 7474–7484.

(51) Hoy, R. S.; Robbins, M. O. Effect of equilibration on primitive path analyses of entangled polymers. *Phys. Rev. E* **2005**, *72*, 061802.

(52) Rubinstein, M.; Colby, R. H. *Polymer Physics.* Oxford University Press: Oxford, U.K., 2003.

(53) Salaniwal, S.; Kumar, S. K.; Douglas, J. F. Amorphous solidification in polymer-platelet nanocomposites. *Phys. Rev. Lett.* **2002**, *89*, 258301.

(54) Knauert, S. T.; Douglas, J. F.; Starr, F. W. The effect of nanoparticle shape on polymer-nanocomposite rheology and tensile strength. *J. Polym. Sci., Part B* **2007**, *45*, 1882.

(55) Uchida, N.; Grest, G. S.; Everaers, R. Vicoelasticity and primitive path analysis of entangled polymer liquids: From factin to polyethylene. *J. Chem. Phys.* **2008**, *128*, 044902.

(56) Kim, J. M.; Keffer, D. J.; Kröger, M.; Edwards, B. J. Rheological and entanglement characteristics of linear chain polyethylene liquids in planar couette and planar elongational flows. *J. Non-Newtonian Fluid Mech.* **2008**, *152*, 168–183.